RESEARCH MEMORANDUM

LONGITUDINAL STABILITY, CONTROL EFFECTIVENESS, AND DRAG CHARACTERISTICS AT TRANSONIC SPEEDS OF A ROCKET-PROPELLED MODEL OF AN AIRPLANE CONFIGURATION HAVING AN UNSWEPT TAPERED WING OF ASPECT RATIO 3.0 AND NACA 65A004.5 AIRFOIL SECTIONS

By John C. McFall, Jr. and James A. Hollinger

Langley Aeronautical Laboratory
Langley Field, Va.

NATIONAL ADVISORY COMMITTEE
FOR AERONAUTICS

WASHINGTON

January 20, 1953

NATIONAL ADVISORY COMMITTEE FOR AERONAUTICS

RESEARCH MEMORANDUM

LONGITUDINAL STABILITY, CONTROL EFFECTIVENESS, AND DRAG CHARACTERISTICS AT TRANSONIC SPEEDS OF A ROCKET-PROPELLED MODEL OF AN AIRPLANE CONFIGURATION HAVING AN UNSWEPT TAPERED WING OF ASPECT RATIO 3.0 AND NACA 65A004.5 AIRFOIL SECTIONS

By John C. McFall, Jr. and James A. Hollinger

SUMMARY

A flight investigation has been conducted on an airplane configuration mounting an unswept tapered wing of aspect ratio 3.0 with NACA 65A004.5 airfoil sections. Static and dynamic longitudinal stability, control effectiveness, and drag characteristics were obtained. Comparisons are presented between the model in the present investigation and similar models mounting wings of the same plan-form dimensions but having hexagonal airfoil sections.

For models having wings of the same material, the NACA 65A004.5 airfoil model had lower values of lift-curve slope than that of the hexagonal airfoil section model. Some nonlinearity in the static stability of the complete configuration was observed at high subsonic speeds. The sharp static stability variations for all models at Mach numbers between 0.90 and 0.95 were indicated to be plan-form effects. The portion of the total airplane normal force carried by the exposed wing was approximately constant over the Mach number range from 0.73 to 1.33. Some buffeting of the model was indicated at high subsonic speeds at lift coefficients only a little below maximum. The zero-lift drag of the wing on this configuration was only a small part of the total model drag. The drag rise of the model occurred at a Mach number of approximately 0.9.

INTRODUCTION

The rocket-propelled airplane configuration model flown in this investigation is the third model, in a general longitudinal-stability

research program, mounting a wing of aspect ratio 3.0, with 16° swept quarter chord and taper ratio 0.40. The wing in this investigation differed from the two models previously flown by having NACA 65A004.5 airfoil sections rather than hexagonal airfoil sections (ref. 1). The data obtained were analyzed by the methods presented in the initial report of this program (ref. 2). The results presented are those obtained from analysis of the model response to deflections of the horizontal tail which was moved in an approximate square-wave program. The longitudinal stability, control effectiveness, and drag characteristics of the configuration were determined from the flight time histories for a Mach number range of 0.73 to 1.33. The model was flown at the Pilotless Aircraft Research Station, Wallops Island, Va.

SYMBOLS

C_N	normal-force coefficient $\left(a_n/g \frac{W/S}{q}\right)$
C_c	chord-force coefficient $\left(-a_l/g \frac{W/S}{q}\right)$
C_L	lift coefficient $(C_N \cos \alpha - C_c \sin \alpha)$
C_D	drag coefficient $(C_c \cos \alpha + C_N \sin \alpha)$
$C_{m_{total}}$	total pitching-moment coefficient
C_{N_W}	wing normal-force coefficient
C_{N_A}	complete-model normal-force coefficient
a_n	normal acceleration as obtained from accelerometer, ft/sec^2
a_l	longitudinal acceleration as obtained from accelerometer, ft/sec^2
g	acceleration of gravity, ft/sec^2
l	distance between accelerometers, ft
p	free-stream static pressure, lb/sq ft
l_t	distance between model c.g. and tail center of pressure, ft

p_o	standard sea-level static pressure (2116 lb/sq ft)
$\bar{c}$	wing mean aerodynamic chord, ft
$b_e/2$	exposed wing semispan, ft
c	wing chord, ft
G	torsional modulus of elasticity, lb/sq in.
y	lateral distance from fuselage center line, ft
m_θ	wing torsional stiffness parameter, in.-lb/radian
m	couple applied near wing tip, in.-lb
θ	local wing twist angle produced by m, radians; or angle of pitch, deg
α	angle of attack, deg
δ	elevator deflection, deg
M	Mach number
S	wing area (including the area enclosed within the fuselage), sq ft
W	weight, lbs
q	free-stream dynamic pressure, lb/sq ft
I_y	moment of inertia in pitch, slug-ft^2
P	period of oscillation, sec
R	Reynolds number, based on wing mean aerodynamic chord
$T_{1/2}$	time to damp to one-half amplitude, sec
$\ddot{\theta}$	pitching acceleration, deg/sec^2
γ	flight-path angle, deg
$\dot{\gamma}$	$d\gamma/dt$

Subscripts:

T	trim
$\dot{\alpha}$	$(d\alpha/dt)(\bar{c}/2V)(1/57.3)$
q	$(d\theta/dt)(\bar{c}/2V)$
W	wing
A	complete model
F	fuselage
t	tail

MODELS AND APPARATUS

Models

The model used in this investigation is the third in a general research program to investigate thin unswept wings of aspect ratio 3. This model is referred to in this paper as model C. The general model dimensions are presented in figure 1, and three photographic views of the configuration are shown in figure 2. For comparison purposes, information is included herein on the two thin unswept-wing models from reference 1, which are referred to as models A and B. The three models were closely similar and differed only in the following respects: wing airfoil and material, fuselage length, and vertical tail.

Models A and B had wings of hexagonal section and model C had a wing with NACA 65A004.5 airfoil sections. The material of construction of the wings was steel for model A and aluminum for models B and C. Model C had two inches of additional fuselage length in the cylindrical part of the fuselage ahead of the wing. The tail of model C had an extra vertical fin added below the fuselage to prevent the erratic behavior of longitudinal oscillations mentioned in the analysis section of reference 3. The all-movable horizontal tail was deflected from 1.10° to -1.95° in an approximate square wave pattern. A detailed description of models A and B is presented in reference 1. Model C weighed 131.2 pounds, had a moment of inertia about the axis of pitch of 12.84 slug-feet square, and had its center of gravity at 12.5 percent of the mean aerodynamic chord.

Instrumentation

The model was equipped with a 10-channel telemeter to transmit data from the model during flight. The continuously recorded measurements were as follows: two normal accelerations, longitudinal acceleration, transverse acceleration, angle of attack, two wing normal-force measurements, control position, total-head pressure, and static pressure. The normal accelerations were measured at the center of gravity and at the nose to provide a measurement of pitching acceleration. The wing was mounted on a beam-type balance from which wing normal forces were measured. One wing normal-force gage was an inductance type of gage used previously on another model (ref. 4) and the other was a strain-gage type installed for development purposes only. A vane-type angle-of-attack indicator was mounted on a sting protruding from the nose of the model (ref. 5). The total-pressure tube was located on a small strut below the fuselage. The static pressure was measured from a calibrated orifice located 4.9 inches behind the beginning of the cylindrical portion of the fuselage.

Radar tracking units were used to obtain model range and elevation, and Doppler velocimeter radar recorded velocity against time. Radiosondes measured atmospheric conditions at the time of the flight. Fixed and manually operated 16-millimeter motion-picture cameras were used to photograph the launching of the model and the first portion of the flight.

Preflight Measurements

The torsional-stiffness characteristics of the wing were determined by applying a couple at the tip and measuring the twist at several sections. The results are shown in figure 3. The factor plotted, Gc_{tip}^3/m_θ, is a nondimensional parameter which makes the result a direct function of wing shape only. For use in comparing the aeroelastic properties of this wing with other results the value of free-stream static pressure, as obtained in the model flight, divided by standard sea-level pressure is presented in figure 4 as a function of Mach number.

For use in analyzing the test results for buffet information the model was subjected to vibrations of known frequency, in order to obtain the response of telemeter instruments in the model and vibrational characteristics of major components, such as wing, tail, or nose.

Measurements were made of the weight of the moving parts of the wing balance and wing panels. These measurements were used in applying a correction for inertia effects on the wing-balance readings by the method of reference 4.

At values of wing normal force above 800 pounds the wing root displacement was stopped by the fuselage because of fuselage flexibility.

[redacted]

This resulted in incorrect values of wing normal-force readings obtained from the deflection of the wing-balance inductance-gage instrument. For this reason, the values of wing normal force obtained from high-lift oscillations were not used for the wing-alone lift-curve slopes nor for the ratios of wing lift to airplane lift. Any reference to wing-alone data in this report includes interference.

TESTS AND ANALYSIS

Tests

The model was launched at an elevation of approximately 60° from a hydraulically elevated mobile launcher as shown in figure 2(c). The model contained no rocket motor and was boosted to maximum velocity by a 6-inch-diameter ABL Deacon solid-fuel rocket motor. Drag separation of the model from the booster followed booster burnout by reason of the different drag-weight ratios of the model and booster.

The scale of the test is shown in figure 5(a), where Reynolds number is plotted as a function of Mach number.

Analysis

The data were analyzed for the decelerating portion of the flight after model separation from the booster. A small correction for rate of pitch was applied to the indicated angles of attack to convert them to angles of attack at the center of gravity of the model (ref. 5). The wing normal-force measurements were corrected for inertia effects by the method of reference 4.

Each abrupt movement of the horizontal tail produced a short-period oscillation in a_n, α, and a_l, which damped during the time that the horizontal tail remained fixed, and from these quantities C_L and C_D were reduced. Analysis of the period, damping, and trim angle of attack using the equations of motion for two degrees of freedom yields the desired aerodynamic parameters. A detailed presentation of this method of analysis is made in appendix A of reference 2.

The additional instrumentation used in this investigation but not used in reference 1 was a wing normal-force balance and a normal accelerometer in the nose. The values from the wing balance were used for obtaining wing-alone normal-force coefficients and wing contribution to the total lift. The normal accelerometer in the nose was used, together with the normal accelerometer at the center of gravity, to obtain pitching acceleration used in the following equation:

$$C_{m_{total}} = \frac{I_y \ddot{\theta}}{qS\bar{c}}$$

where

$$\ddot{\theta} = \frac{g}{l}\left[(a_n/g)_{nose} - (a_n/g)_{cg}\right]$$

The data were recorded continuously on the telemeter record for all channels but, for the purpose of plotting and reduction of data, readings of the telemeter record were made at intervals of 0.01 second. All slopes were taken from plots of the first 1 or $1\frac{1}{2}$ cycles of each oscillation. Periods, damping, and trim values were determined from plots of entire oscillations.

ACCURACY

Previous experience has shown the accuracy of telemetered measurements to be 2 percent of the full-scale calibrated range of the instrument. The following table gives estimated values of the possible systematic errors in the absolute values of C_{N_A}, C_c, and C_{N_W}, as affected by the instrument calibration ranges.

M	qS	W/qS	C_{N_A}	C_c	C_{N_W}
1.30	6470	0.0203	0.018	0.0028	0.026
1.10	4620	.0284	.026	.0040	.037
.80	2240	.0587	.053	.0082	.077

A consideration of all the factors involved indicates that the Mach numbers are accurate to ±1 percent at supersonic speeds and ±2 percent at subsonic speeds. Further errors in the aerodynamic coefficients may arise from possible dynamic-pressure inaccuracies which are approximately twice as great as the errors in Mach number.

The errors in the measured angles of attack and horizontal-tail deflections, being independent of dynamic pressure, are not likely to vary with Mach number. The horizontal-tail deflections are estimated to be accurate to ±0.1° and the increments in angle of attack to ±0.2°.

RESULTS AND DISCUSSION

Lift Limit and Buffeting

The lift information and range of buffeting, analyzed by using vibrational characteristics of the model, are summarized in figure 5(b). Some additional buffet information at lower Mach numbers is presented in figure 5(c) as angle-of-attack variation rather than lift coefficient because of the low values of normal force and the consequent decreased accuracy of the lift coefficient at the lower Mach numbers. A similar variation with Mach number of the boundary for unsteady air flow to that experienced by the model between $M = 0.6$ and $M = 0.7$ was found for thin airfoils in the study of fluctuating pressures on two-dimensional airfoils in reference 6 and was attributed to leading-edge flow attachment.

Lift

The lift curves obtained over the Mach number range from $M = 0.7$ to $M = 1.3$ for this investigation are presented in figure 6. The data points shown are those reduced from the telemeter record at time intervals of 0.01 second. The lift coefficients are plotted against angle of attack for the first $1\frac{1}{2}$ cycles of each oscillation. Difference in lift at a given angle of attack in figure 6 is shown by symbols representing increasing and decreasing angle of attack. This difference was found to be of smaller magnitude for the round-nose airfoil in the present investigation than for models A and B in reference 1.

The average lift-curve slope of model C is shown in figure 7 plotted against Mach number along with the lift-curve slopes of models A and B (ref. 1). The data points shown in figure 7 represent points from the faired lines presented in figure 6. The variation of lift-curve slope with Mach number was similar for all models, with model C having a lower value than model B which was of the same material of construction.

The lift effectiveness of the all-movable horizontal tail $\Delta C_L/\Delta\delta$, presented in figure 8 for model C, are in good agreement with the values given for models A and B, which were shown to be of the right order of magnitude in reference 1. The break in the curve for model C results from absence of trim data at the trim change for the high-lift tail setting.

Wing normal-force coefficients plotted against total configuration normal-force coefficients during low-lift oscillation are presented in figure 9. The high-lift oscillation data are not presented for the reason given in the section entitled "Preflight Measurements." The wing

normal-force coefficients were determined from the telemetered data at 0.01-second time intervals. Some difference is noted for increasing or decreasing angle of attack.

The rate of change of wing normal-force coefficient with total configuration normal-force coefficient is presented in figure 10 plotted against Mach number. The values obtained indicate that the wing contribution to the total lift is approximately constant over the Mach number range $M = 0.7$ to $M = 1.3$. The ratio of exposed to total wing area compared with the values of $dC_{N_W}/dC_{N_{WF}}$ indicates that the fuselage lift is in proportion to the wing area enclosed within the fuselage. The value $dC_{N_W}/dC_{N_{WF}}$ was obtained by using the values of dC_{N_W}/dC_{N_A} from figure 9 where dC_{N_A} has been corrected for tail lift (ref. 1) which is shown as dC_{N_t}/dC_{N_A}. A comparable value of $dC_{N_W}/dC_{N_{WF}}$ may be found in reference 7 where for a wing of aspect ratio 3 a similar wing-body combination at a Mach number of 0.25 had a value of $\frac{C_{N_{\alpha_W}}}{C_{N_{\alpha_{WF}}}} = 0.74$.

Drag

Figure 11 presents the minimum drag coefficients of model C, and the round-nose and hexagonal-airfoil section drag models (ref. 8). The drag rise for model C occurred at a Mach number of 0.9. The drag for models A and B is not presented, since the configurations differed from Model C by the absence of the additional vertical fin and by having different wing airfoil sections. A comparison of model C with the wingless model in reference 1 shows that the wing contribution to the total drag is only a small part of the total drag of the configuration. The difference in the minimum drag coefficients for the drag models (fig. 11) indicates an appreciable effect of airfoil shape. A comparison of the effect of lift on drag (fig. 12) shows lower values for model B when compared with model C as might be expected from the higher values of lift-curve slope for model B. No difference in chord force with angle of attack is indicated by the values of $dC_D/dC_L{}^2$, since the values are nearly equal to the value for no leading-edge suction, $\frac{1}{57.3\ C_{L_\alpha}}$.

The maximum lift-drag ratios for models B and C are plotted against Mach number in figure 13. Also presented in figure 13 are the lift-drag ratios obtained by using minimum drag values including induced drag from the drag models (ref. 8). The magnitude of the $(L/D)_{max}$ values obtained by using the minimum drag of the drag models (ref. 8) is representative of an airplane with a very low fuselage drag.

In figure 14 are presented the lift coefficients at which maximum lift-drag ratios occur for models B and C.

Static Stability

The measured periods of oscillations of angle of attack for model C is shown in figure 15. The data converted to the static stability derivative C_{m_α} at a center of gravity of 12.5 percent of the mean aerodynamic chord and C_{m_α} for models A and B at the same center of gravity are presented in figure 16. A similar variation of C_{m_α} with Mach number of models A, B, and C indicates that the sharp variation between $M = 0.90$ and $M = 0.95$ were plan-form effects. Above $M = 1.0$ model C had a smoother variation of C_{m_α} with Mach number than models A and B.

The variation of the aerodynamic-center location with Mach number for models A, B, and C is shown in figure 17. The same trend is observed for all three models with model C having a smoother variation with Mach number above $M = 1.0$ when compared with models A and B.

The values of pitching-moment coefficient obtained by using the two normal accelerometers presented in figure 18, have been corrected for damping by the following formula:

$$C_m(\alpha) = C_{m_{total}} - \left(C_{m_{\dot{\theta}}} + C_{m_{\dot{\alpha}}}\right)\dot{\alpha} - C_{m_{\dot{\theta}}}\dot{\gamma}$$

where

$$C_{m_{\dot{\theta}}} = C_{m_\delta}\frac{l_t}{V}$$

and $C_{m_{\dot{\theta}}} + C_{m_{\dot{\alpha}}}$, $\dot{\gamma}$, $\dot{\alpha}$, $C_{m_{total}}$, and C_{m_δ} are obtained from the flight data. The faired lines shown are those obtained from the readings of the periods. Some of the pitching-moment-coefficient curves when plotted against time did not oscillate about a mean value of zero, probably because of small errors in the readings of either or both of the normal accelerometers. When this situation occurred, the curves were shifted to produce a mean value of zero, as required by the equilibrium conditions.

Damping in Pitch

The time to damp to one-half amplitude plotted against Mach number is presented in figure 19. The data converted to damping coefficient $C_{m_q} + C_{m_{\dot{\alpha}}}$ and plotted against Mach number are shown in figure 20 for

models A, B, and C. No difference in damping coefficient for different tail deflection was noted for models A and B. The reason for the disagreement in damping coefficient between models A and B and model C is not known but the same sharp variation at $M = 0.8$ to $M = 0.9$ has been observed in similar configurations with different wings (refs. 3 and 4). These differences between models were not observed in static stability.

Longitudinal Trim and Control Effectiveness

The variation of trim lift coefficient and the trim angle of attack with Mach number for the two control positions are shown in figures 21(a) and 21(b), respectively. No abrupt changes were apparent in either quantity with Mach number.

The variation of the change in trim angle of attack per degree change in horizontal-tail deflection with Mach number is presented in figure 22 for models A, B, and C. Good agreement was obtained among the models for this quantity as well as for change in trim lift coefficient per degree change in horizontal-tail-deflection variation with Mach number shown in figure 23.

CONCLUSIONS

The flight investigation over the Mach number range from 0.75 to 1.3 of an airplane configuration having a thin unswept wing of aspect ratio 3 and NACA 65A004.5 airfoil sections indicated the following conclusions:

1. The variation of lift-curve slope was similar for the model having an NACA 65A004.5 airfoil section and similar models with hexagonal airfoil sections. The model with the NACA 65A004.5 airfoil section had a lower value of lift-curve slope than a model with a wing of the same material but with hexagonal airfoil section.

2. The part of the total airplane normal force carried by the exposed wing was approximately constant over the Mach number range from 0.73 to 1.23. The fuselage lift was in proportion to the wing area enclosed within the fuselage.

3. Buffeting of the model occurred at high subsonic speeds at lift coefficients only a little below the maximum.

4. The zero-lift drag of the wing of this configuration was only a small part of the total-model drag. The drag rise for the model occurred at a Mach number of approximately $M = 0.9$.

5. The static stability of the complete configuration varied with lift coefficient at subsonic speeds. A similar variation of static stability with Mach number for both hexagonal and NACA 65A004.5 airfoil section wing models indicated that the sharp variations at Mach numbers between 0.90 and 0.95 were plan-form effects.

Langley Aeronautical Laboratory,
National Advisory Committee for Aeronautics,
Langley Field, Va.

REFERENCES

1. Gillis, Clarence L., and Vitale, A. James: Wing-On and Wing-Off Longitudinal Characteristics of an Airplane Configuration Having a Thin Unswept Tapered Wing of Aspect Ratio 3, As Obtained From Rocket-Propelled Models at Mach Numbers From 0.8 to 1.4. NACA RM L50K16, 1951.

2. Gillis, Clarence L., Peck, Robert F., and Vitale, A. James: Preliminary Results From a Free-Flight Investigation at Transonic and Supersonic Speeds of the Longitudinal Stability and Control Characteristics of an Airplane Configuration With a Thin Straight Wing of Aspect Ratio 3. NACA RM L9K25a, 1950.

3. Chapman, Rowe, Jr., and Morrow, John D.: Longitudinal Stability and Drag Characteristics at Mach Numbers From 0.70 to 1.37 of Rocket-Propelled Models Having a Modified Triangular Wing. NACA RM L52A31, 1952.

4. Vitale, A. James, McFall, John C., Jr., and Morrow, John D.: Longitudinal Stability and Drag Characteristics at Mach Numbers From 0.75 to 1.5 of an Airplane Configuration Having a 60° Swept Wing of Aspect Ratio 2.24 As Obtained From Rocket-Propelled Models. NACA RM L51K06, 1952.

5. Mitchell, Jesse L., and Peck, Robert F.: An NACA Vane-Type Angle of Attack Indicator for Use at Subsonic and Supersonic Speeds. NACA RM L9F28a, 1949.

6. Humphreys, Milton D.: Pressure Pulsations on Rigid Airfoils at Transonic Speeds. NACA RM L51I12, 1951.

7. Hopkins, Edward J., and Carel, Hubert C.: Experimental and Theoretical Study of the Effects of Body Size on the Aerodynamic Characteristics of an Aspect Ratio 3.0 Wing-Body Combination. NACA RM A51G24, 1951.

8. Morrow, John D., and Nelson, Robert L.: Large-Scale Flight Measurements of Zero-Lift Drag of 10 Wing-Body Configurations at Mach Numbers From 0.8 to 1.6. NACA RM L52D18a, 1953.

[redacted]

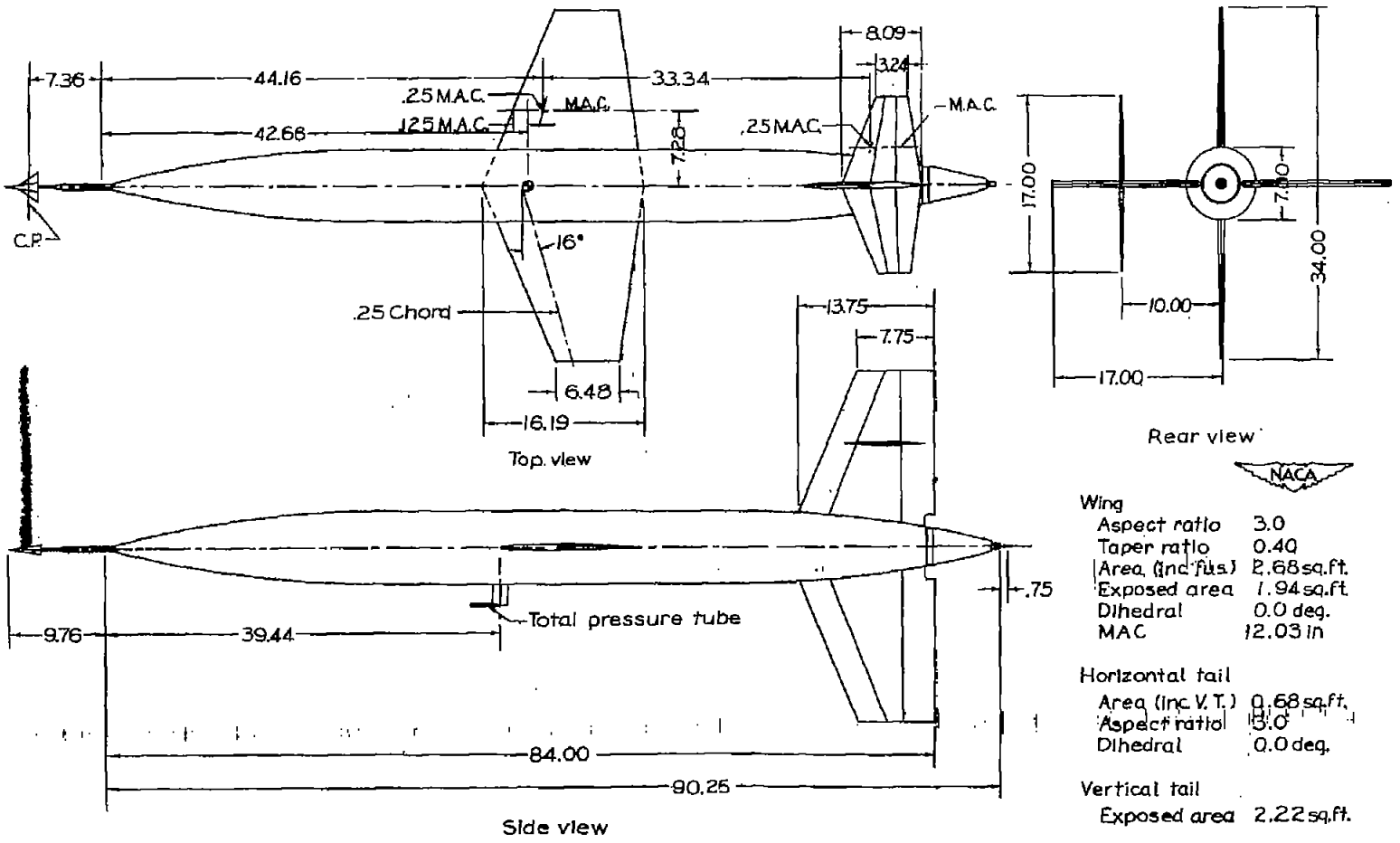

Figure 1.- General arrangement of model. All dimensions in inches.

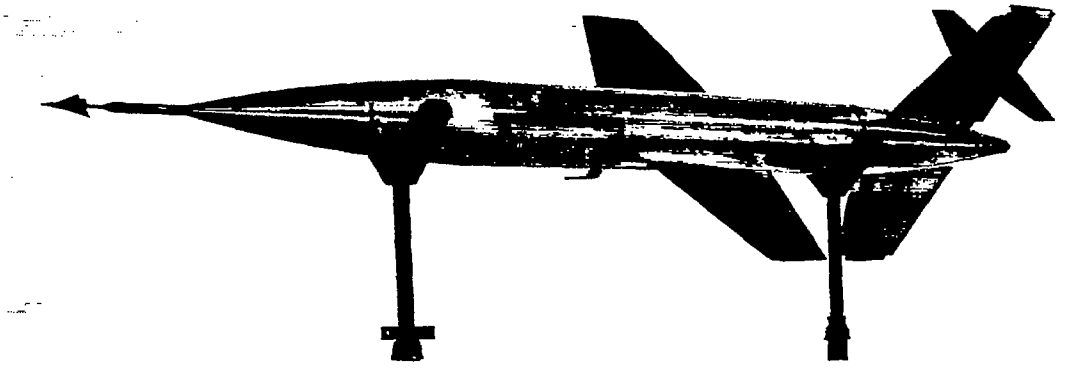

(a) Three-quarter front view. L-70958

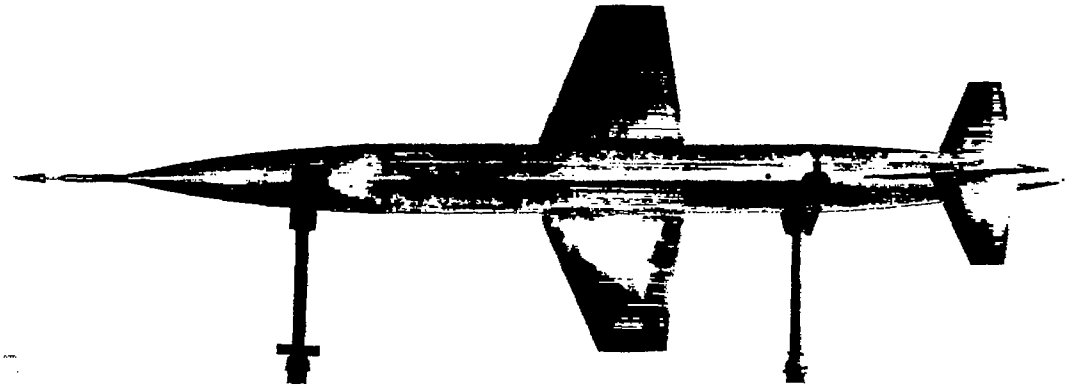

(b) Top view. L-70955

Figure 2.- Photograph of configuration investigated.

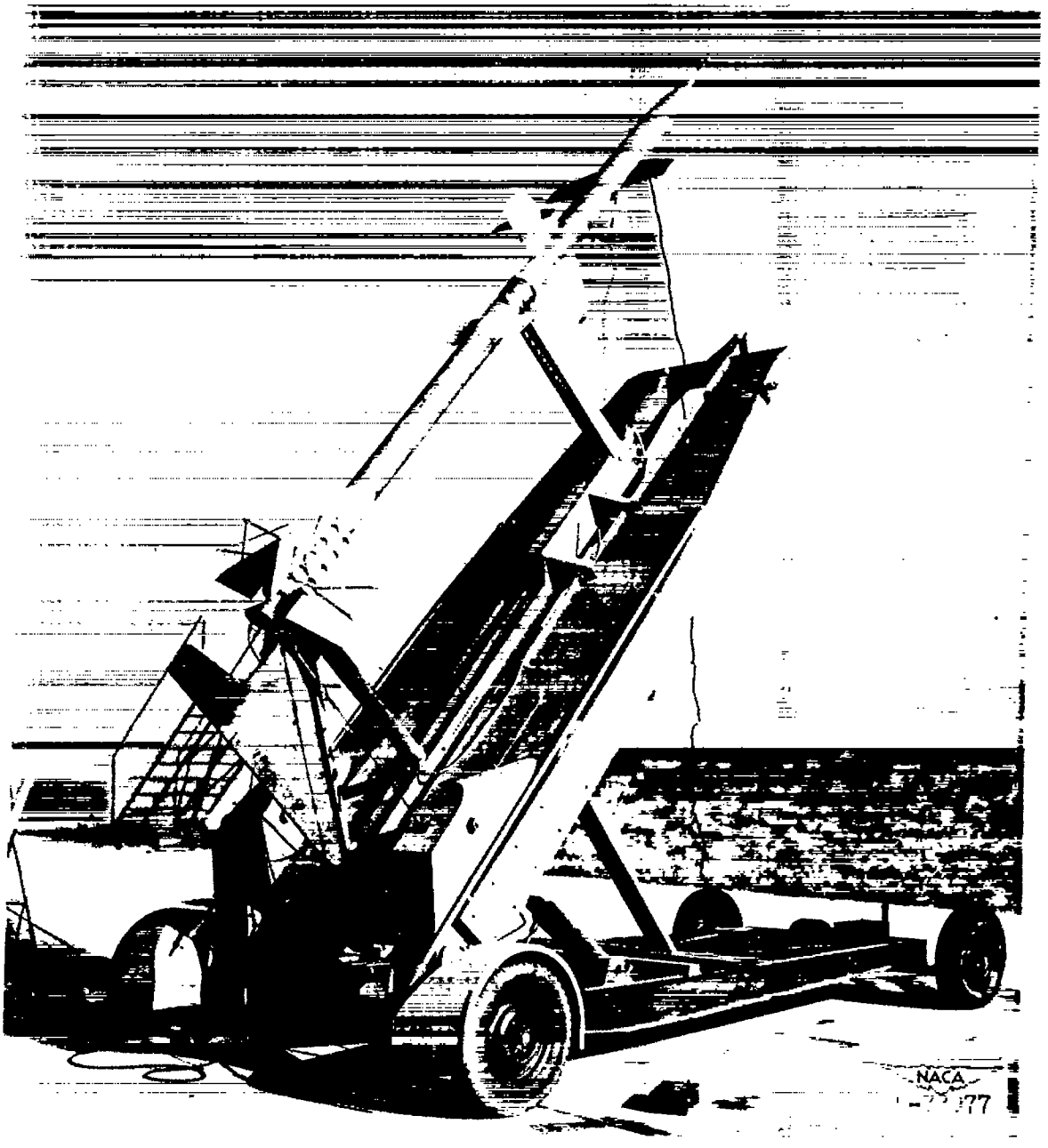

(c) Model on launcher.

Figure 2.- Concluded.

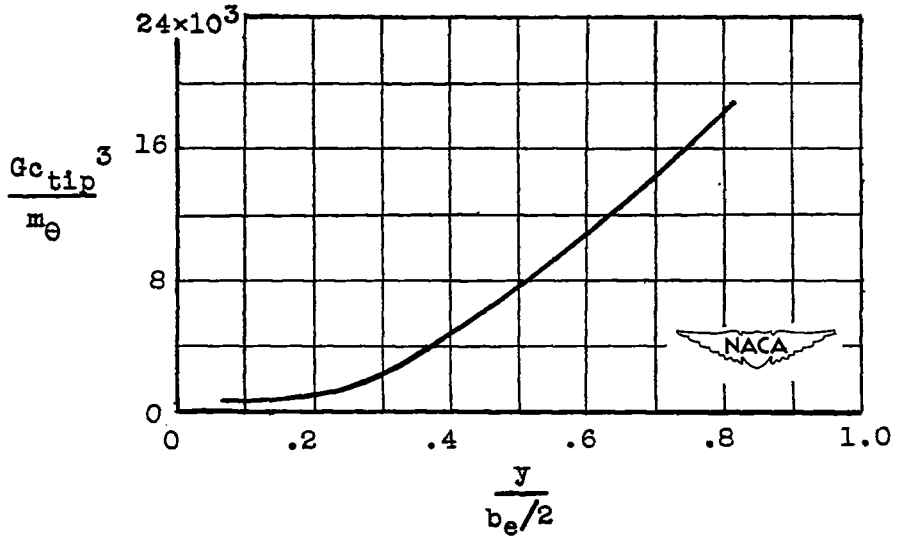

Figure 3.- Measured torsional rigidity of the wing.

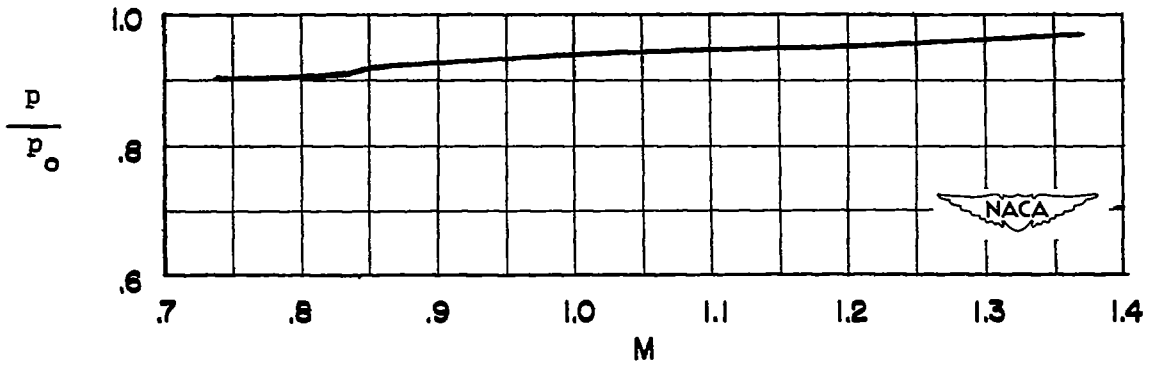

Figure 4.- Variation of static-pressure ratio with Mach number.

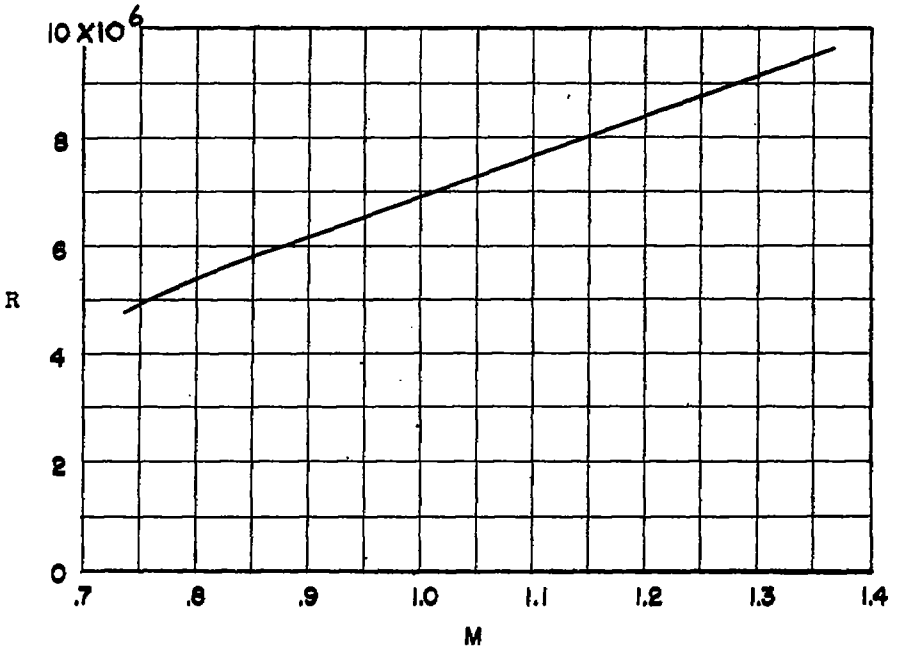

(a) Reynolds number based on wing mean aerodynamic chord.

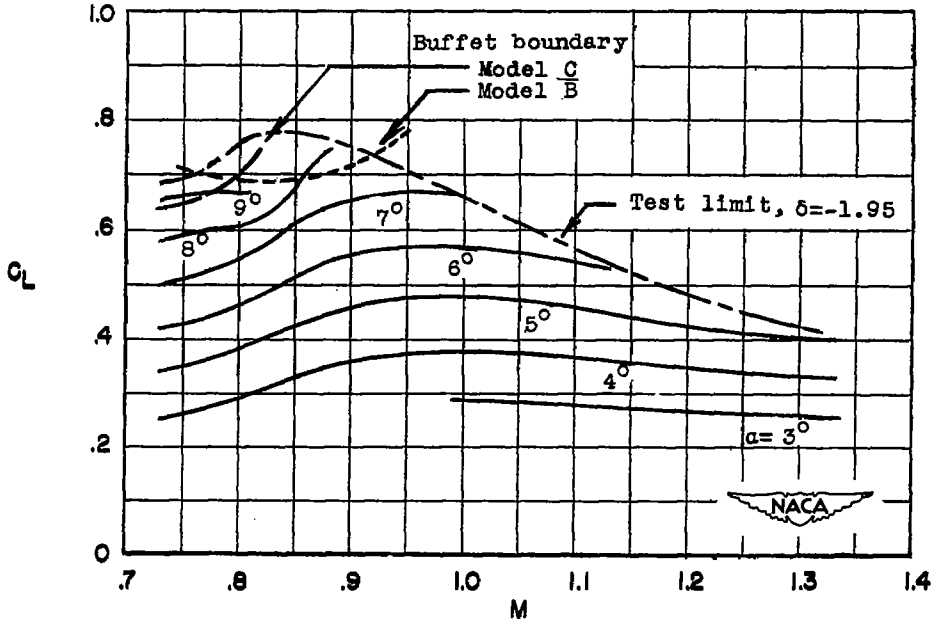

(b) Lift and buffet information. $\delta = -1.95^{\circ}$.

Figure 5.- Range of tests.

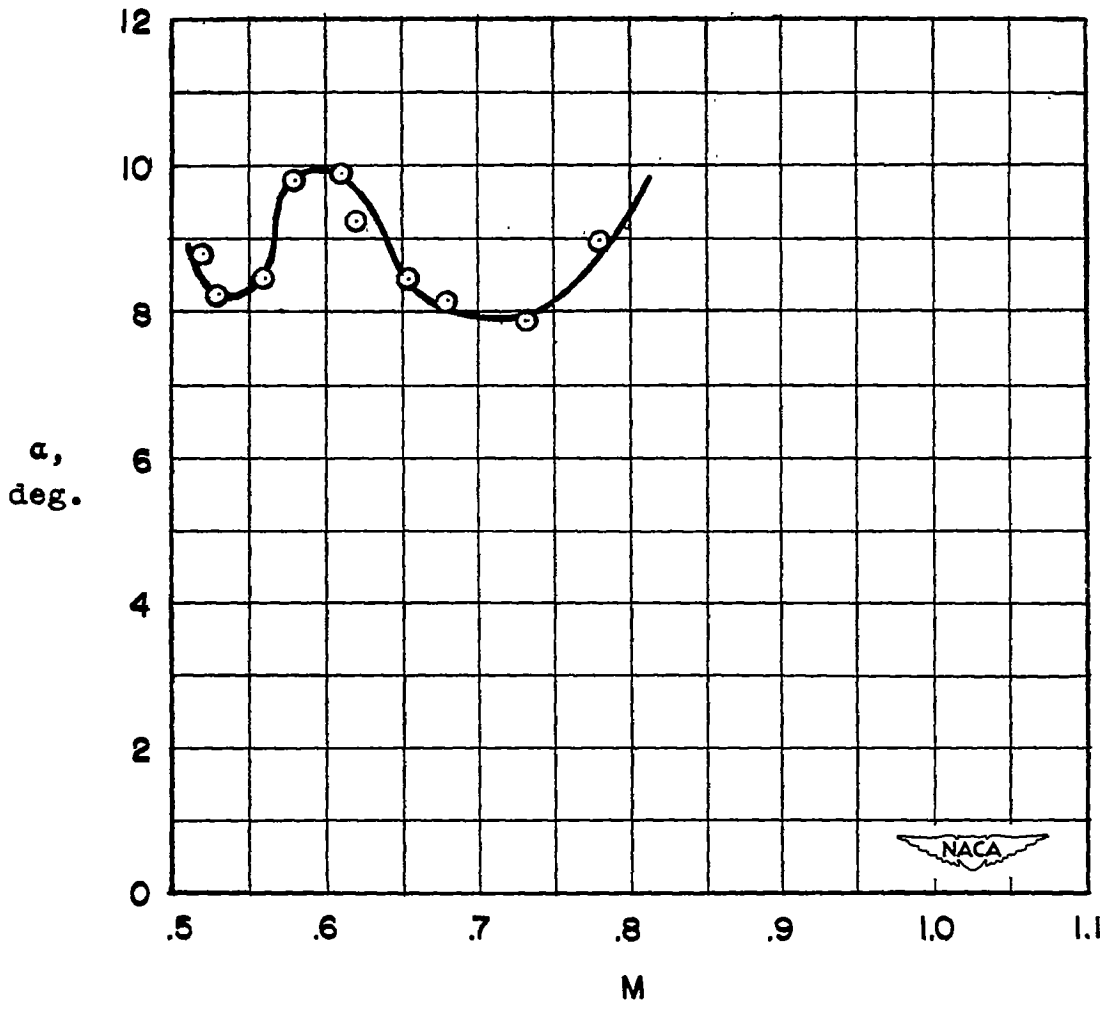

(c) Variation with Mach number of angle of attack at which buffeting first occurred.

Figure 5.- Concluded.

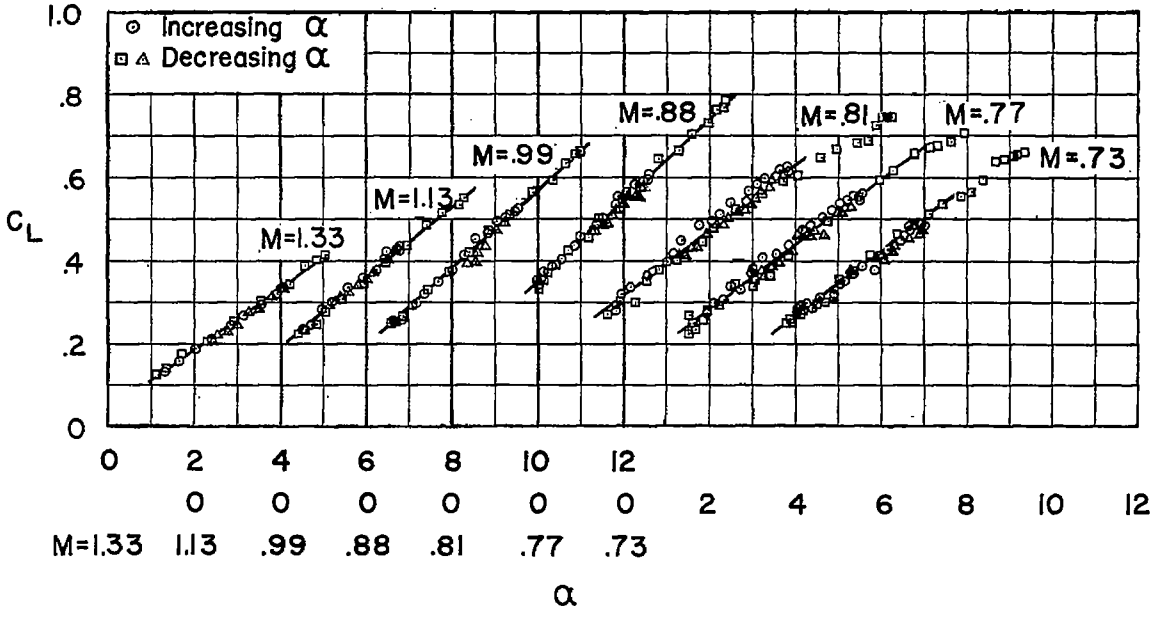

(a) δ = -1.95.

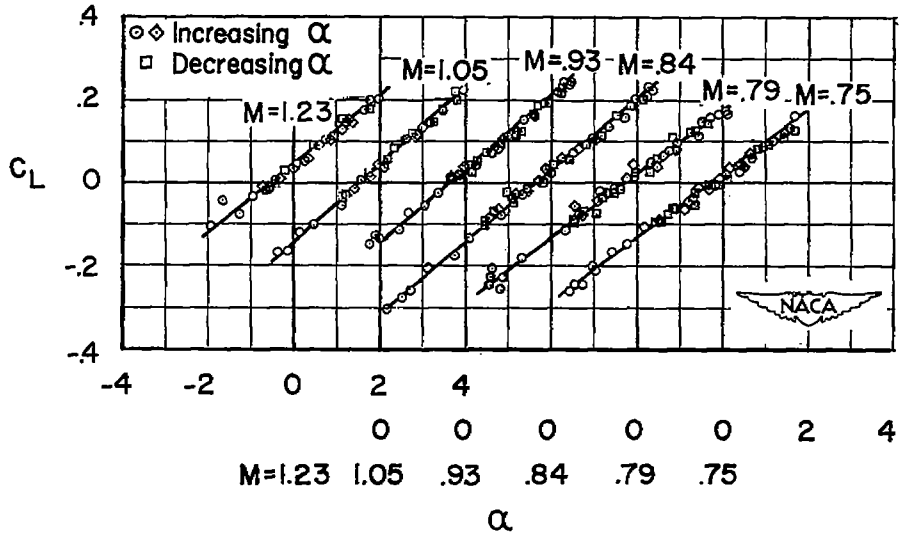

(b) δ = 1.10.

Figure 6.- Variation of lift coefficient with angle of attack.

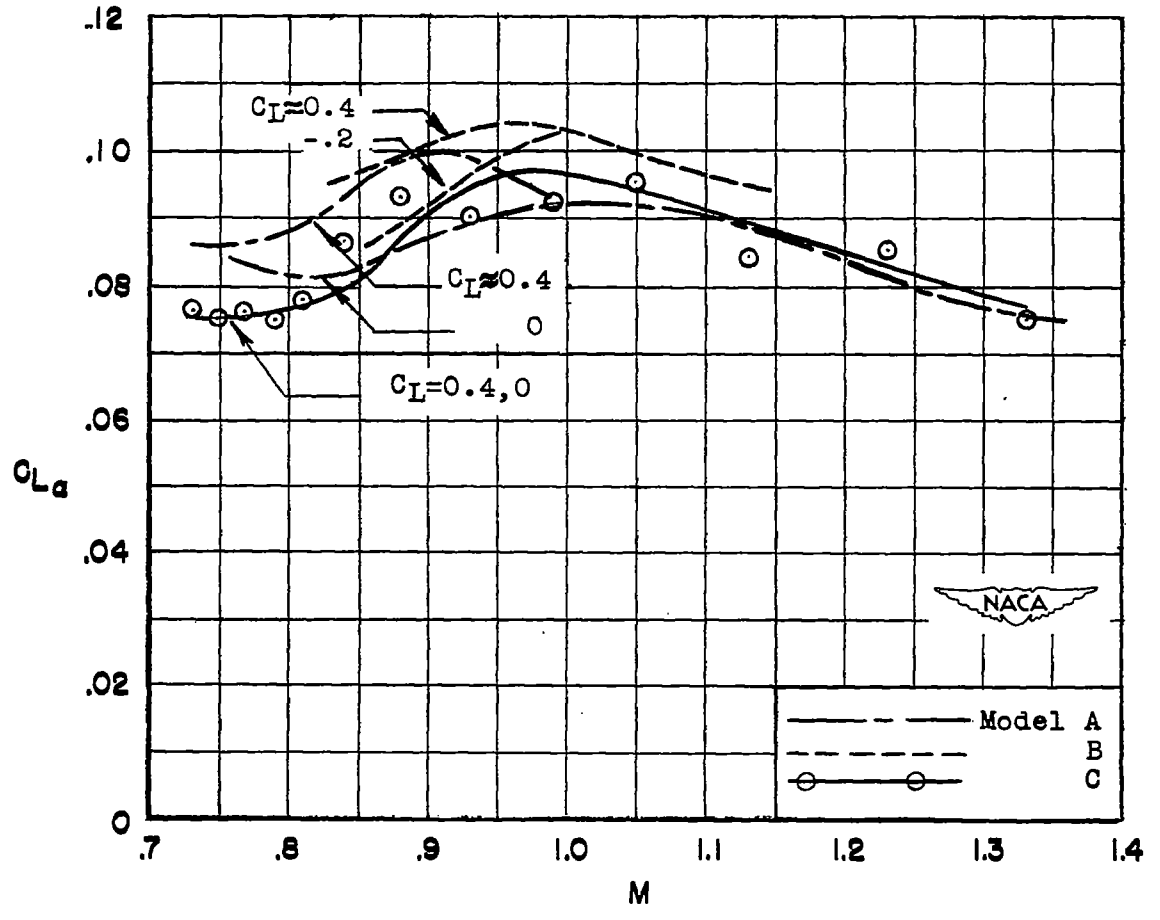

Figure 7.- Lift-curve slope of complete model.

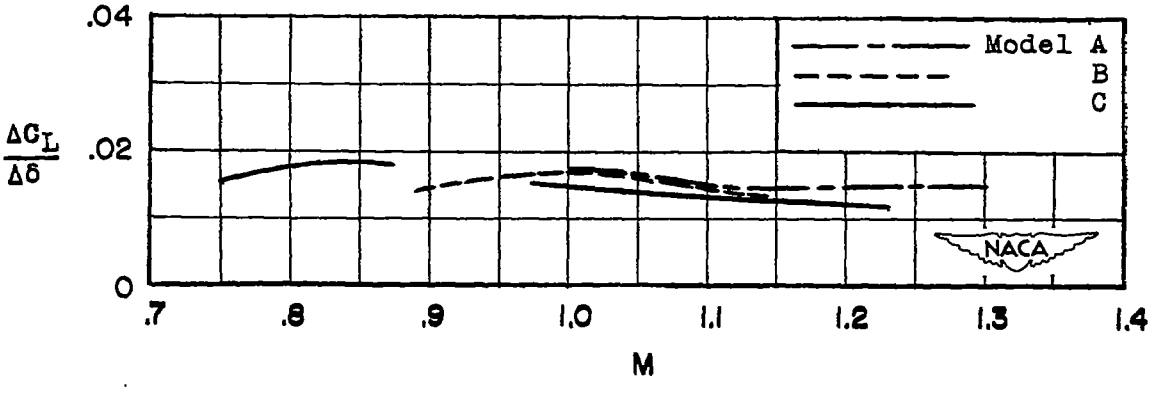

Figure 8.- Lift effectiveness of horizontal tail.

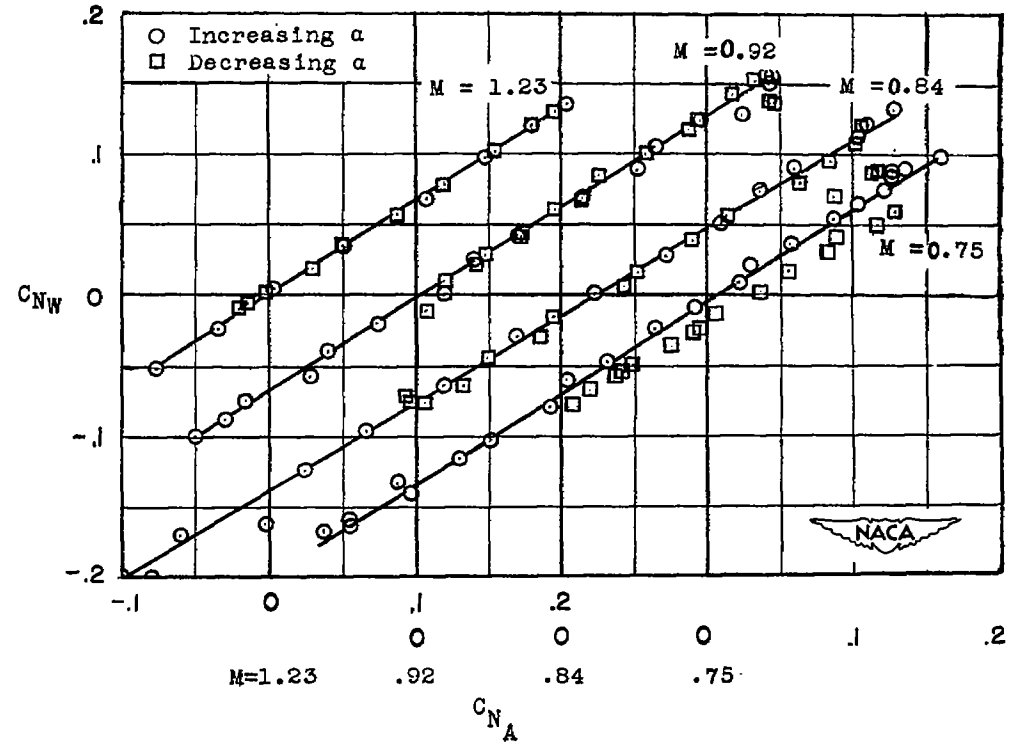

Figure 9.- Variation of wing normal-force coefficient with airplane normal-force coefficient during several typical oscillations.

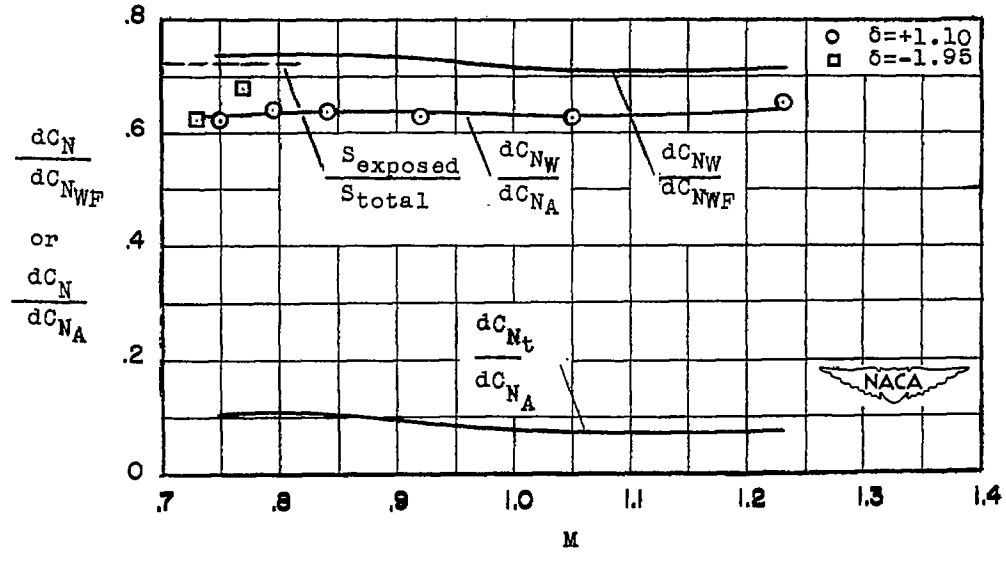

Figure 10.- Rate of change of wing normal-force coefficient with airplane normal-force coefficient.

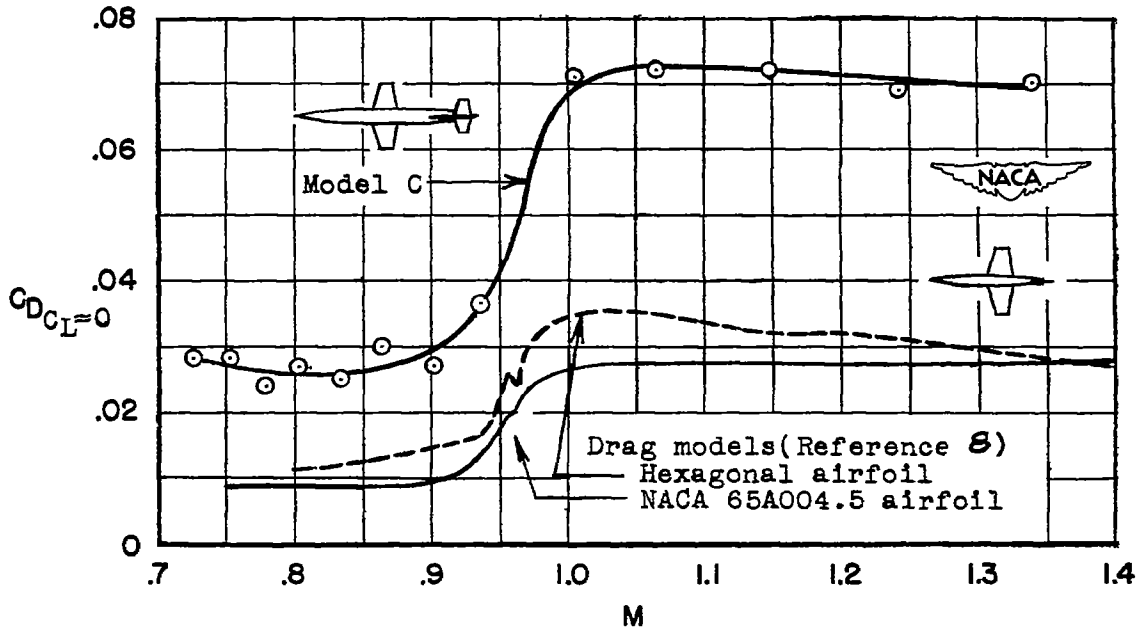

Figure 11.- Minimum drag coefficients of complete models.

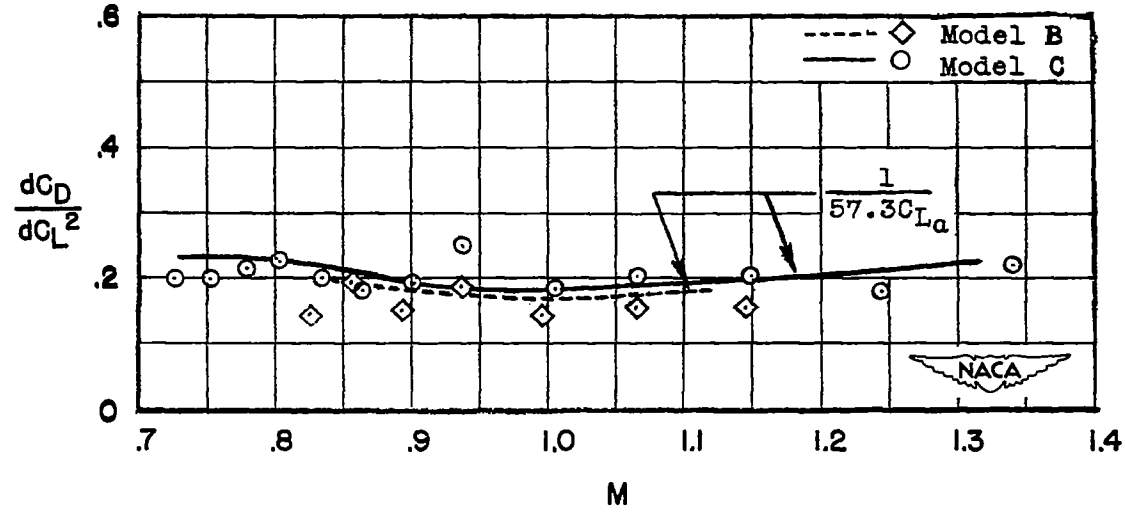

Figure 12.- Effect of lift on drag.

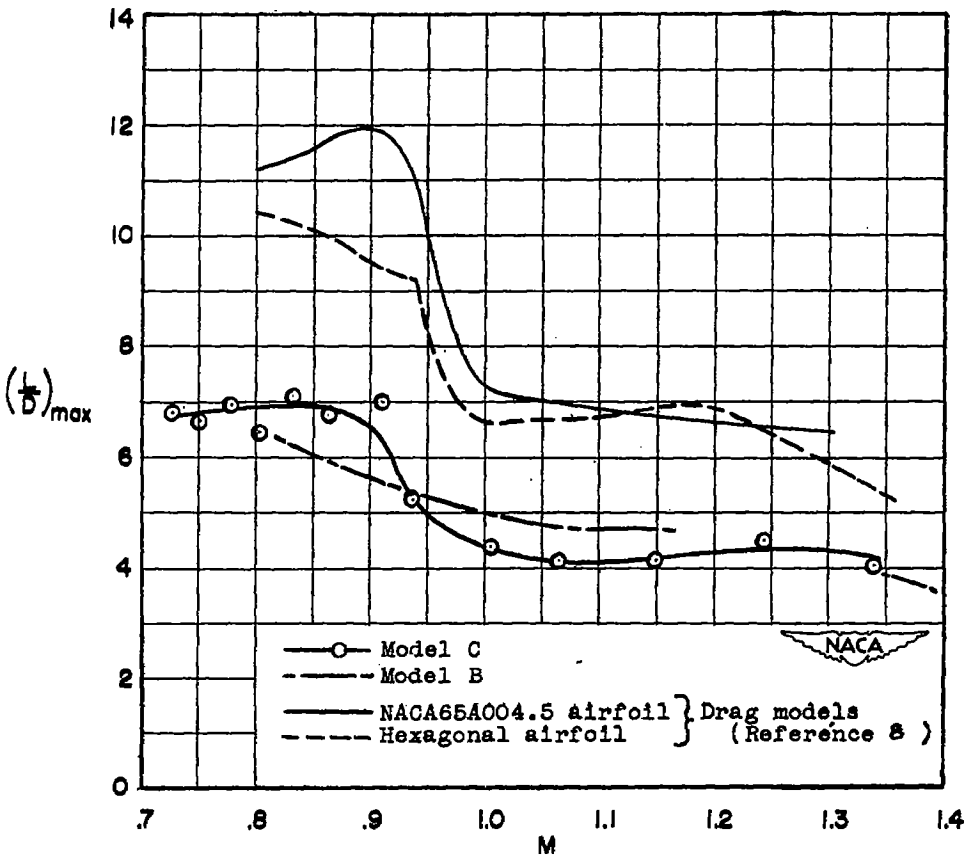

Figure 13.- Maximum lift drag ratios.

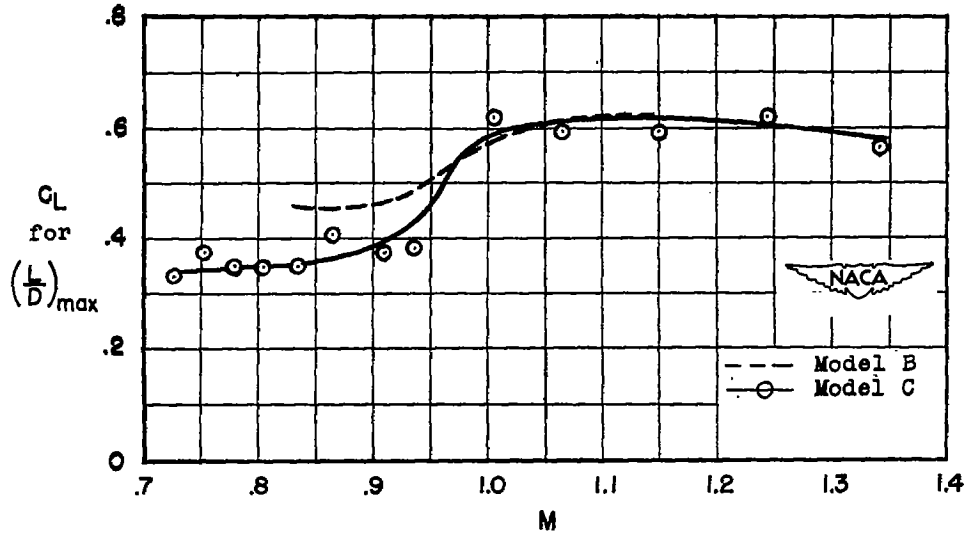

Figure 14.- Lift coefficients for maximum lift-drag ratio.

[redacted]

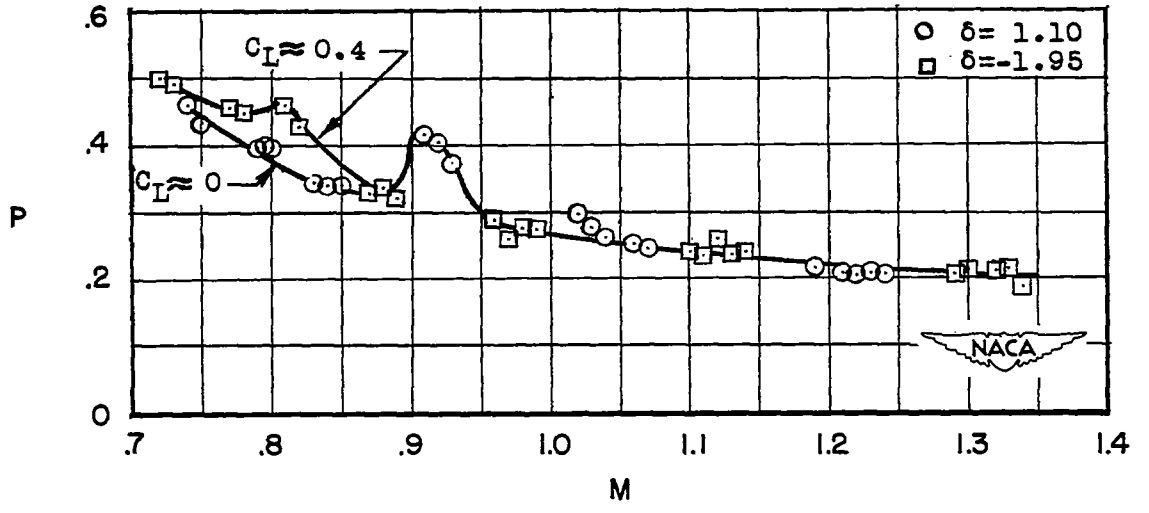

Figure 15.- Period of oscillations.

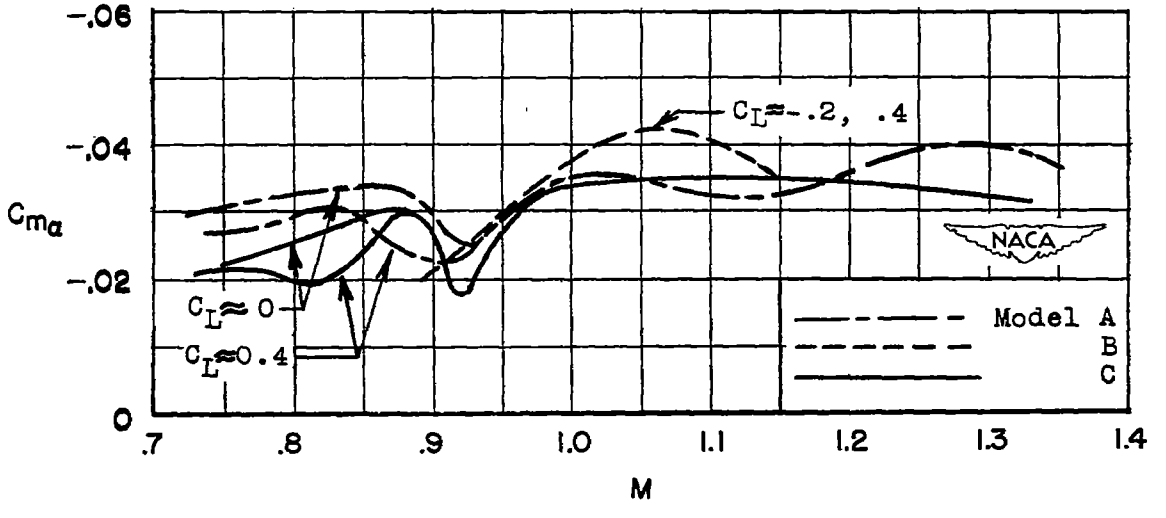

Figure 16.- Static stability of complete models. Center of gravity at 12.5 percent mean aerodynamic chord.

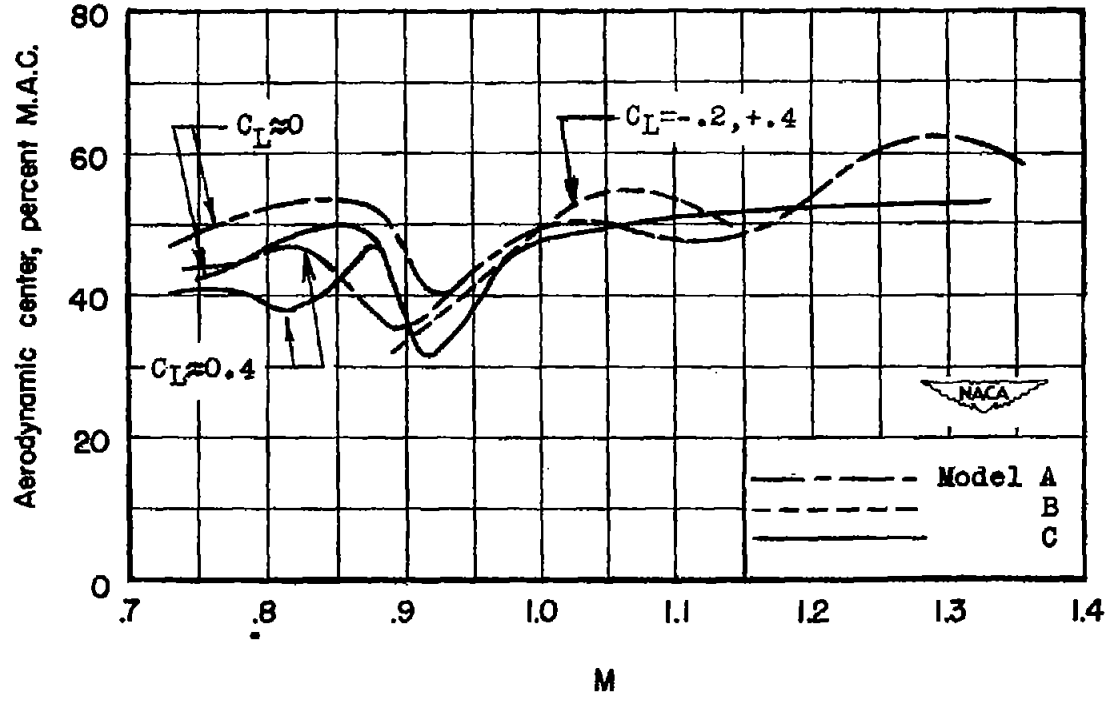

Figure 17.- Aerodynamic-center location.

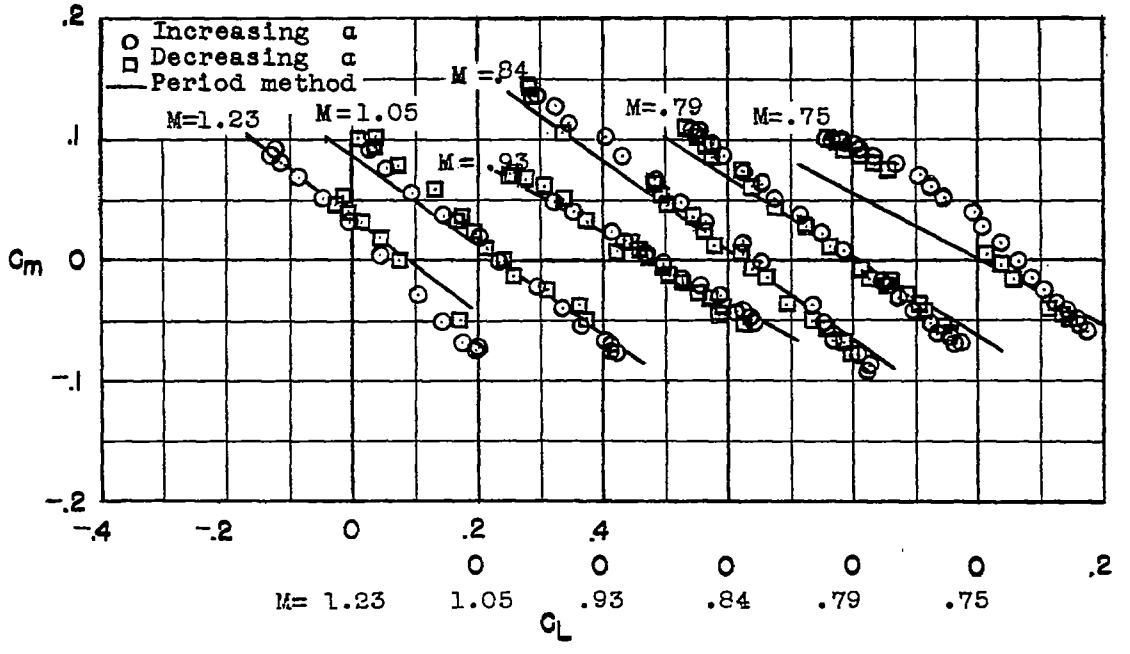

(a) $\delta = 1.10$.

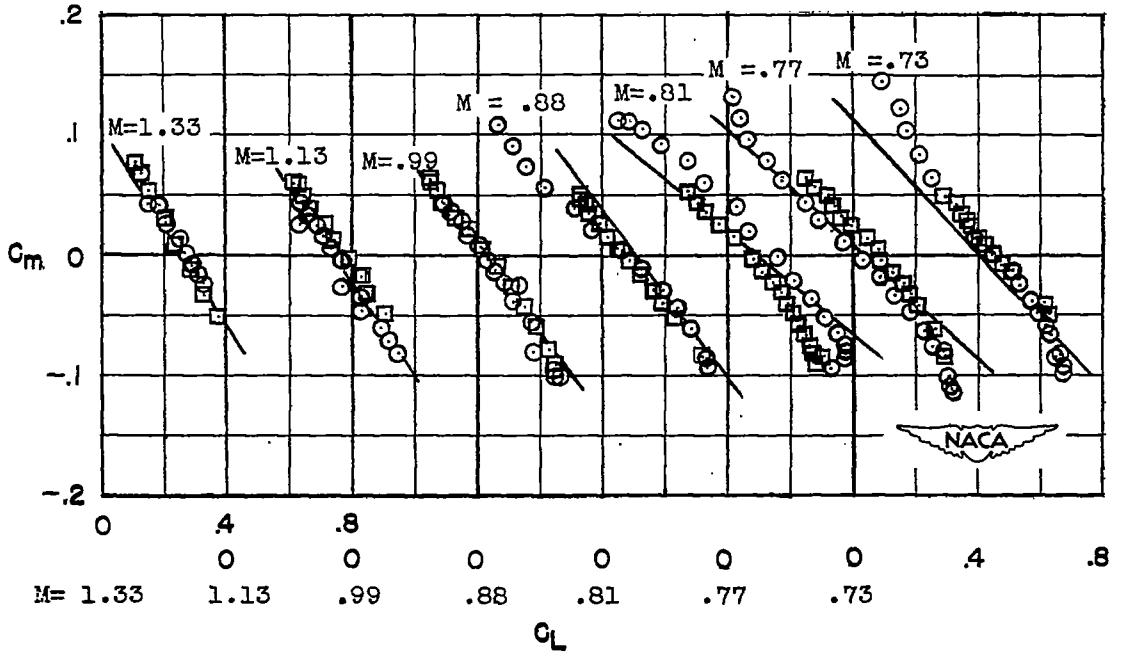

(b) $\delta = -1.95$.

Figure 18.- Variation of pitching-moment coefficient with lift coefficient.

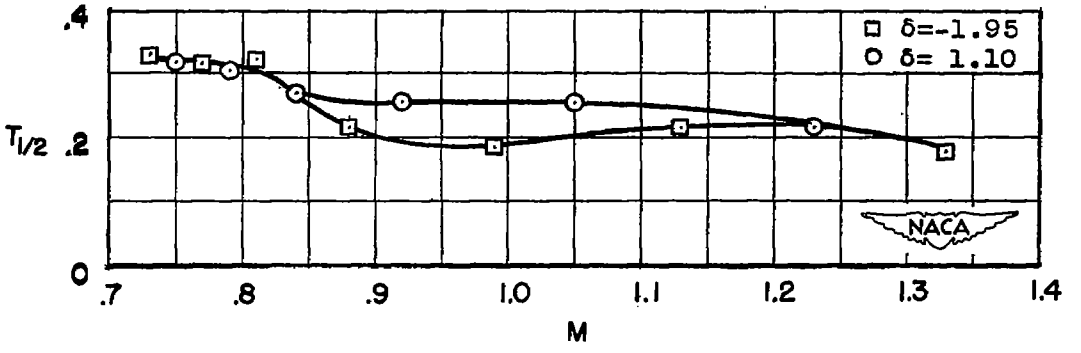

Figure 19.- Time to damp to one-half amplitude.

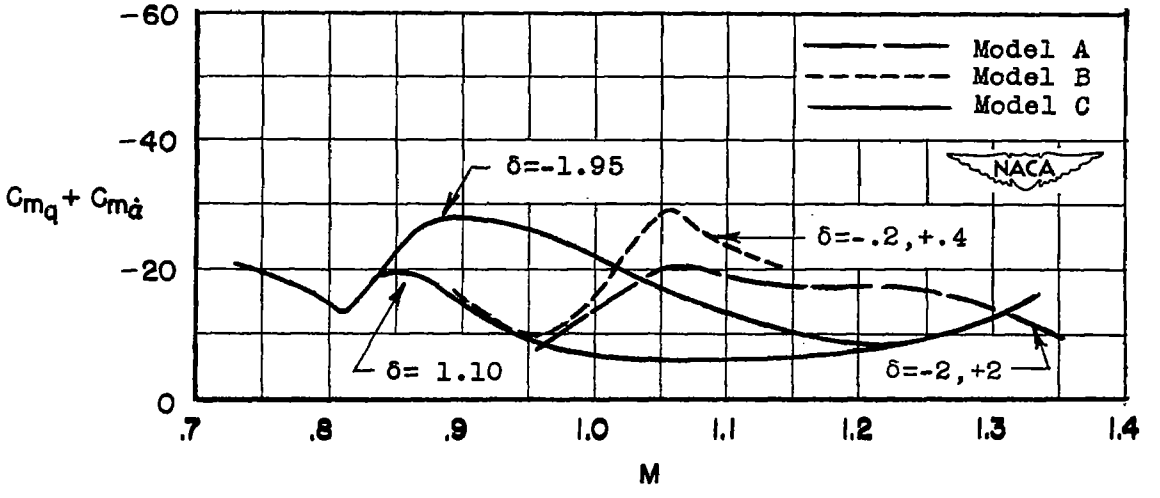

Figure 20.- Damping derivative.

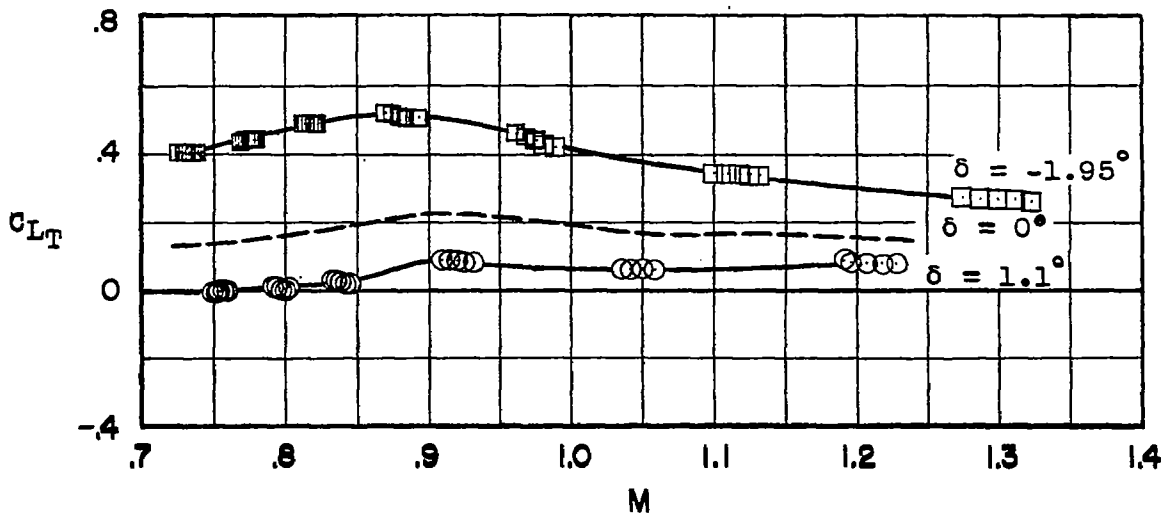

(a) Trim lift coefficient.

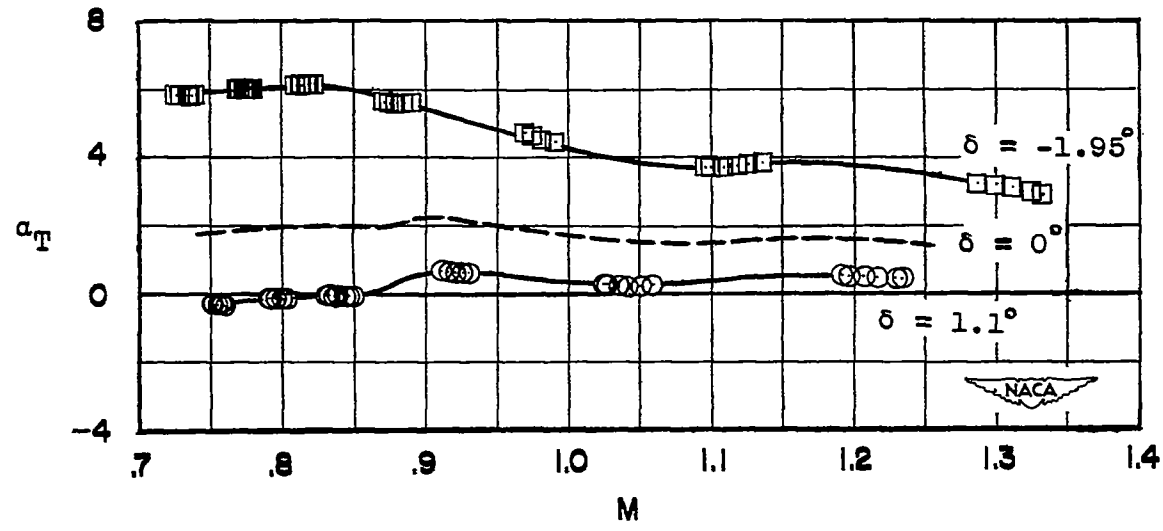

(b) Trim angle of attack.

Figure 21.- Trim characteristics.

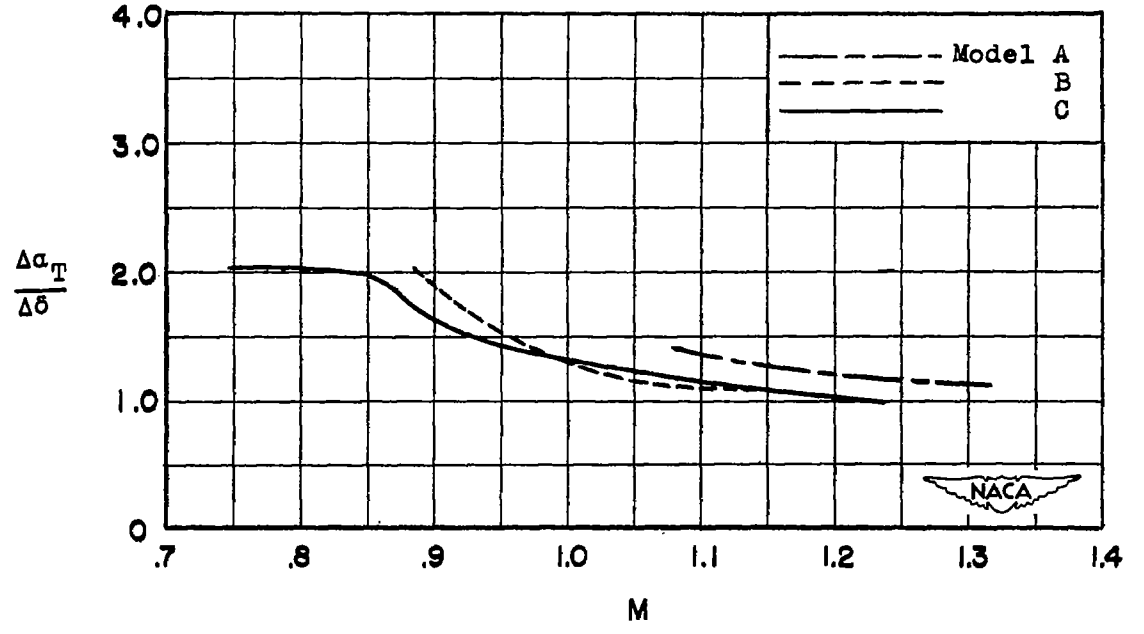

Figure 22.- Change in trim angle of attack per degree change in horizontal tail deflection.

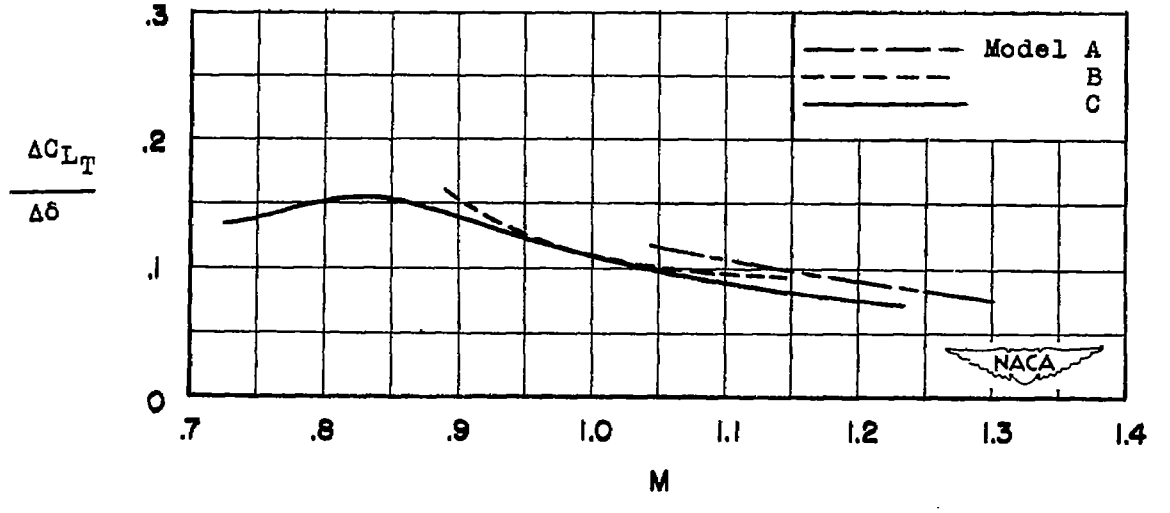

Figure 23.- Change in trim lift coefficient per degree change in horizontal tail deflection.